Pulsed-power volume-heating chemical vapor infiltration

José I. Morell, Demetre J. Economou,[a] and Neal R. Amundson
Department of Chemical Engineering, University of Houston, Houston, Texas 77204-4792

(Received 12 December 1991; accepted 18 May 1992)

The dynamic behavior of a novel chemical vapor infiltration (CVI) technique called pulsed-power volume-heating CVI is investigated using a diffusion-reaction model. In this technique, a volume-heating source (e.g., RF or microwave) is used to heat the preform. The source power is modulated in time (e.g., square-wave modulation) with a specific period and duty cycle. During the low-power part of the cycle, the temperature of the composite drops, reducing the reaction rate and thus allowing the precursor gas to diffuse into the composite, essentially "refilling" the composite. This alleviates reactant concentration gradients within the composite minimizing density nonuniformities. The high-power part of the cycle is used to achieve rapid reaction rates, thereby minimizing processing time. CVI of a carbon fiber preform with carbon resulting from methane decomposition is taken as an example to illustrate the technique. The results reveal the dependence of density uniformity and processing time on relevant variables such as pulse period, duty cycle, power density level, and methane mole fraction. It is shown that pulsed-power volume-heating CVI can provide a window of operating conditions leading to rapid and complete densification.

I. INTRODUCTION

Fiber-reinforced ceramic composites are being investigated extensively because they possess vital properties required in a large number of high temperature structural applications.[1] Ceramic composites consist of two distinct phases: a ceramic matrix that spans the whole composite and a continuous or discontinuous fibrous reinforcement. The introduction of a fibrous reinforcement is critical in order to overcome the inherent brittleness of monolithic ceramics which can lead to catastrophic failure. Ceramic composites are characterized by their increased fracture toughness, reliability, durability, and noncatastrophic failure.

Chemical vapor infiltration (CVI) has emerged as one of the most promising techniques for the fabrication of fiber-reinforced ceramic composites.[2,3] Advantages of CVI are its ability to synthesize solids with fine grain microstructure at relatively low temperatures, to fabricate components of complex shape, and to produce a wide range of composites. In CVI, gaseous precursors are transported into a heated preform by diffusion and/or forced flow where they react to deposit a solid film. Gaseous byproducts diffuse out of the preform and are removed by an exhaust system. Complete densification and short processing time are important goals of any CVI process. Traditional constant temperature (isothermal) CVI suffers from nonuniform deposition and long processing times that may reach several weeks. In order to alleviate some of these difficulties, other types of operation have been proposed including the thermal gradient, isothermal-forced flow, thermal gradient-forced flow, and pulsed flow CVI.[4]

Mathematical modeling of CVI helps understanding of the physicochemical processes involved in the infiltration process. This understanding can be used to pinpoint the direction for process improvements. In addition, mathematical models can be used to identify optimum operating conditions, to evaluate novel reactor configurations, and to establish process control strategies. Several investigators have reported on the modeling of CVI processes. Middleman[5] and Sheldon[6] showed that proper selection of the system chemistry may lead to process improvements. Melkote and Jensen[7] used Monte Carlo simulations to describe the evolution of the structural parameters of the composite. They studied the effect of temperature under isothermal and temperature-gradient conditions. Recently, pulsed-pressure CVI was studied by Sotirchos[8] employing a model to describe the dynamic behavior of the process.

Extensive research is being conducted to assess the impact of volume heating in the processing of ceramics. Volume heating is attractive because it can offer lower processing times, fast response to changes in power, and the potential to produce ceramics with particular microstructural properties. Volume heating can be achieved by using microwave power[9] for dielectric materials or radio frequency induction in the case of conductive composites. A mathematical model for volume-

[a]Author to whom correspondence should be addressed.

heating CVI was proposed by Gupta and Evans.[10] They investigated CVI of SiC with microwave heating and external cooling. The authors used a simplified model of the preform structure (a single pore model) and did not consider the transient nature of the composite temperature as densification progresses.

A comprehensive model of CVI with volume heating has recently been developed by Morell *et al.*[11] In this investigation, a detailed description of the multicomponent nature of the mass transport processes and of the evolving pore structure was included along with constitutive equations describing the transport-reaction processes. Model results revealed the existence of a critical value of power density above which entrapment of accessible porosity occurs. Several step-function power modulation schemes were proposed to achieve rapid and complete densification. These modulation schemes, however, require the determination of appropriate power level(s) and switching time(s) in order to obtain optimum results.

In the present study, a mathematical model is developed for a novel technique called pulsed-power volume-heating CVI. In this technique the power of the volume-heating source (microwaves or RF) is modulated according to a given waveform. A square-wave modulation is examined in this paper, but other waveforms (e.g., sinusoidal or sawtooth) may be applied. The pulsed-power volume-heating technique has the following advantages: (1) volume heating results in a favorable temperature profile with highest temperature at the center of the preform and monotonically decreasing temperature toward the edges; (2) during the low-power part of the cycle, the average temperature of the preform and hence the reaction rate decreases. This allows deeper penetration of the precursor gas within the composite since the lower reaction rate prevents depletion of the gas; (3) during the high-power part of the cycle the reaction proceeds rapidly, thereby minimizing the processing time. The above advantages allow for the development of an "inside-out" densification pattern that results in complete and rapid densification of the preform.

The deposition of carbon in a carbon fiber preform is selected as a model chemical system to explore the general characteristics of the pulsed-power volume-heating technique. The process is described by a set of equations for the space and time dependence of species concentration, temperature, pressure, and porosity. A detailed description of the multicomponent transport processes is included as well. The results reveal the dependence of the system behavior on key parameters and operating conditions. In particular, variations in deposit uniformity and processing time are investigated as a function pulse period, duty cycle, power density level, and methane mole fraction.

II. MODEL FORMULATION

A. Conservation equations

A schematic diagram of the CVI reactor is shown in Fig. 1. The system consists of a cylindrical preform which is heated symmetrically using a microwave or radio frequency apparatus. The source power can be modulated according to a square-wave with variable power levels, period, and duty cycle. The preform consists of cylindrical fibers randomly oriented in three-dimensional space. A gaseous mixture of known composition and temperature flows continuously through the reactor, keeping a constant species concentration at the preform surface. Gaseous precursors (e.g., CH_4) infiltrate the fiber-matrix composite, and at the same time participate in a reaction network resulting in solid deposition that fills the pores of the composite. The temperature distribution in the composite at any time depends on the power absorbed and the density distribution at that time through the combined effects of heat conduction, convection, and radiation. As a result, the system is characterized by the space and time variations of species concentration, temperature, and porosity.

The conservation equation for the rth gaseous species is given by (see list of symbols for meaning of symbols)

$$\epsilon_A C \frac{\partial x_r}{\partial t} + \nabla \cdot \mathbf{J}_r + \mathbf{N} \cdot \nabla x_r = \sum_{i=1}^{n^R} \nu_{ri} R_i - x_r \sum_{r=1}^{n^G} \sum_{i=1}^{n^R} \nu_{ri} R_i \quad (1)$$

where ϵ_A is the accessible porosity, C is the total gaseous concentration, x_r and $\mathbf{J}_r$ are the mole fraction and the diffusive flux of the rth species, respectively, $\mathbf{N}$ is the total molar flux; n^G and n^R are the number of gaseous

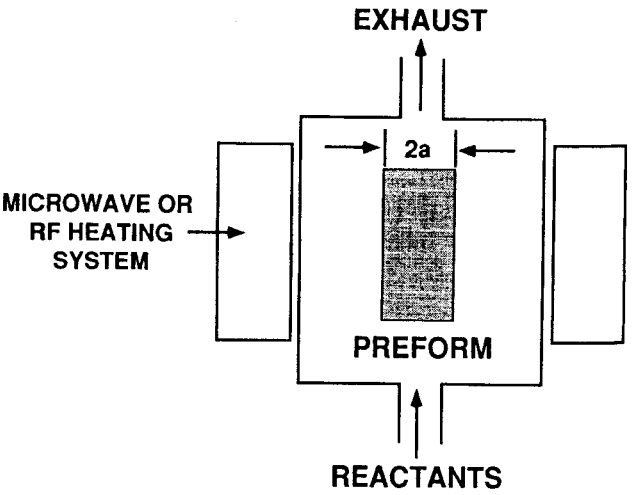

FIG. 1. Schematic diagram of the volume-heating CVI process.

species and chemical reactions considered in the model, and R_i is the rate of the ith reaction per unit volume of composite (solid + voids). The overall conservation equation takes the following form:

$$\frac{\partial(C\epsilon_A)}{\partial t} + \nabla \cdot \mathbf{N} = \sum_{r=1}^{n^G}\sum_{i=1}^{n^R} \nu_{ri} R_i \tag{2}$$

The multicomponent transport processes are described by the Dusty Gas model. This model takes into account that the transport of individual gaseous species within the composite is caused by several mechanisms including molecular diffusion, Knudsen diffusion, and viscous flow. For cases with negligible contributions to the fluxes by surface diffusion, thermal diffusion, and thermal transpiration, the Dusty Gas model can be written as[12]

$$\sum_{s=1}^{n^G} \frac{x_s\mathbf{J}_r - x_r\mathbf{J}_s}{\Delta_{rs}} = -\frac{P}{RT}\nabla x_r - \frac{x_r}{RT}\left(1 - \frac{1}{D_r^e \sum_{s=1}^{n^G} x_s/D_s^e}\right)\nabla P = -A_r \tag{3}$$

$$\mathbf{N} = -\frac{\sum_{s=1}^{n^G} \mathbf{J}_s/D_s^e}{\sum_{s=1}^{n^G} x_s/D_s^e} - \frac{1}{RT}\left(\frac{B_0 P}{\eta} + \frac{1}{\sum_{s=1}^{n^G} x_s/D_s^e}\right)\nabla P \tag{4}$$

where P is total pressure, T is temperature, and D is diffusivity. Δ_{rs} is given by

$$\frac{1}{\Delta_{rs}} = \frac{1}{D_{rs}^e} + \frac{1}{D_r^e D_s^e \sum_{t=1}^{n^G} x_t/D_t^e} \tag{5}$$

The previous equations, in conjunction with the constraint that the sum of the diffusive molar fluxes must be zero, constitute a complete set of independent equations for the molar fluxes in a mixture of n^G species. For a three-component mixture, like the one considered in the present work, solution of the flux equations provides the following explicit expression for the molar fluxes J_r:

$$J_1 = -\Delta_{12}\Delta_{23}\Delta_{31} \times \frac{\{A_1/\Delta_{23} - x_1[A_1(1/\Delta_{23} - 1/\Delta_{12}) + A_2(1/\Delta_{31} - 1/\Delta_{12})]\}}{[x_1(\Delta_{23} - \Delta_{12}) + x_2(\Delta_{31} - \Delta_{12}) + \Delta_{12}]} \tag{6}$$

$$J_2 = -\Delta_{12}\Delta_{23}\Delta_{31} \times \frac{\{A_2/\Delta_{31} - x_2[A_1(1/\Delta_{23} - 1/\Delta_{12}) + A_2(1/\Delta_{31} - 1/\Delta_{12})]\}}{[x_1(\Delta_{23} - \Delta_{12}) + x_2(\Delta_{31} - \Delta_{12}) + \Delta_{12}]} \tag{7}$$

and a similar equation for J_3. The following expression describes temperature variations inside the composite:

$$C_p^e \frac{\partial T}{\partial t} - \nabla \cdot (k^e \nabla T) + \sum_{r=1}^{n^G} (\mathbf{N}_r C_{p_r}) \cdot \nabla T + \sum_{i=1}^{n^R} (\Delta H_i R_i) = (1 - \epsilon)\Phi \tag{8}$$

where C_p^e and k^e are the effective heat capacity per unit volume and effective thermal conductivity of the fiber-matrix composite, respectively. The first term on the left-hand side of Eq. (8) is an energy accumulation term, whereas the second to fourth terms account for conduction, convection, and heat of reaction, respectively. The term on the right-hand side represents the power absorbed by the fiber-matrix composite due to volume heating. Φ is the power absorbed per unit volume of solid. If power is absorbed by the solid phase only, one must multiply by the solid fraction $(1 - \epsilon)$, where ϵ is the total porosity. It was further assumed that power attenuation due to absorption in the solid is negligible. This appears to be a reasonable assumption for thin preforms of materials that do not absorb strongly. Effects of power attenuation in the preform will be examined in the future.

In the pulsed-power volume-heating process, the power varies with time according to a prescribed functionality. In the present study, a square-wave power modulation was examined, as shown in Fig. 2. Important variables of this scheme include the pulse period, t_p, the interval of time in which the high power is on, t_1, the interval of time in which the low power is on, t_2, and the power levels used, Φ_1 and Φ_2. Mathematically, the square-wave power modulation may be represented by the following relations:

$$\tilde{t} = t - t_p \mathrm{Int}(t/t_p) \tag{9}$$

and

$$\Phi = \begin{cases} \Phi_1, 0 \leq \tilde{t} < t_1 \\ \Phi_2, t_1 \leq \tilde{t} < t_p \end{cases} \tag{10}$$

in which $\mathrm{Int}(t/t_p)$ represents the integer part of the ratio t/t_p. In addition, the duty cycle is defined as

$$f_d = \frac{t_1}{t_p} \tag{11}$$

which takes on values between zero and unity.

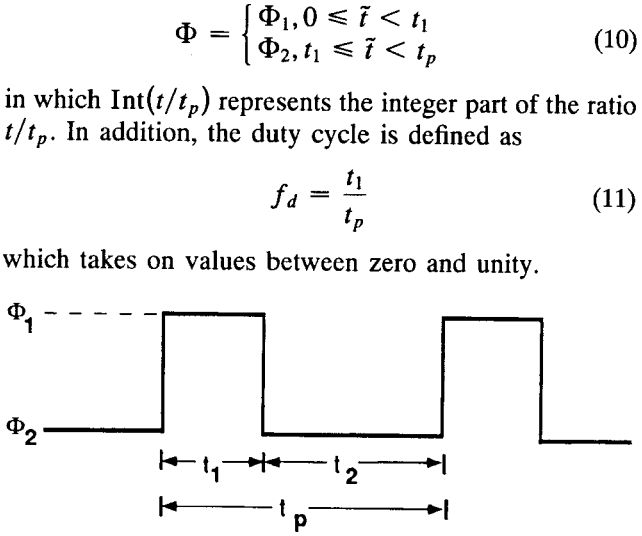

FIG. 2. Square-wave modulation of power.

In order to characterize the densification process, the average trapped accessible porosity, $\bar{\epsilon}_{A,T}$, is introduced as a measure of deposit nonuniformities. This is given by

$$\frac{\bar{\epsilon}_{A,T}}{\epsilon_{A,0}} = \frac{2}{\alpha^2}\int_0^{\alpha}\left(r\frac{\epsilon_{A,T}}{\epsilon_{A,0}}\right)dr \tag{12}$$

where $\epsilon_{A,T}$ represents trapped porosity that can no longer be infiltrated by the reactant. Such a situation occurs, for example, when premature sealing of the pores near the preform surface does not allow reactant to penetrate deeper into the preform, resulting in trapped porosity (which would be accessible otherwise). In Eq. (12), $\epsilon_{A,0}$ is the initial accessible porosity of the preform, r is radial coordinate, and α is the preform radius.

The time and space evolution of the accessible porosity can be obtained from the following equation:

$$\frac{\partial \epsilon_A}{\partial t} = -\frac{M_c}{\rho_C}\sum_{i=1}^{n^R} \nu_{ci} R_i \tag{13}$$

in which M_c and ρ_C are the molecular weight and density of the deposited solid, respectively. In the previous equations, the rate of ith reaction per unit volume of composite, R_i, is given by

$$R_i = \begin{cases} \epsilon_A R_i^*; & \text{for a homogeneous reaction rate} \\ S_A R_{si}; & \text{for a heterogeneous reaction rate} \end{cases} \tag{14}$$

where R_i^* is the reaction rate per unit volume of gas, R_{si} is the reaction rate per unit surface area, and S_A is the accessible surface area per unit volume of composite.

The governing equations are subject to the following boundary and initial conditions:

$$\underline{\text{at } r = 0} \quad \nabla x_r = 0, \qquad \nabla P = 0, \qquad \nabla T = 0 \tag{15}$$

$$\underline{\text{at } r = \alpha} \quad x_r = x_{rb}, \qquad P = P_b,$$
$$-k^e \nabla T = h(T - T_b) + \sigma\tilde{\epsilon}(T^4 - T_b^4) \tag{16}$$

$$\underline{\text{at } t = 0} \quad x_r = x_{r0}, \qquad P = P_0,$$
$$T = T_0, \qquad \epsilon_A = \epsilon_{A,0} \tag{17}$$

Equation (15) is a result of symmetry. Equation (16) implies a constant gas composition and constant pressure at the composite surface. The boundary condition on temperature results by equating the heat losses from the composite surface by the sum of convective (term with heat transfer coefficient h) and radiation (term with Stefan–Boltzmann constant σ) losses. A more detailed description of the model development is given in Ref. 11.

B. Preform structure and model parameters

A comprehensive description of the CVI process requires a realistic representation of the fiber architecture and of the morphological changes that the composite undergoes during infiltration. The spatiotemporal variations of composite structure also make the effective physical and transport properties space and time dependent. In the present study, the cylindrical preform is envisioned as consisting of identical cylindrical fibers randomly positioned in three-dimensional space. The dependence of the diffusion coefficients, surface area, permeability coefficient, and accessible porosity on total porosity for such structure is available in the literature.[13,14]

The transport properties of the multicomponent gaseous mixture were determined using the Chapman–Enskog theory.[15] The mathematical formulation accounts for the dependence of these properties on temperature, pressure, composition, and structural changes of the composite. Temperature dependence and the two-phase nature of the system were accounted for in the calculation of thermodynamic properties.[11]

Our previous study[11] has shown that, under the conditions examined, self-generated pressure variations inside the composite play an insignificant role in determining the behavior of the system. Therefore, the viscous flow contribution to the molar fluxes was neglected [terms involving ∇P in Eqs. (3) and (4) were set equal to zero].

C. Chemical kinetics

In order to gain insight into the pulsed-power volume-heating technique, deposition of carbon by decomposition of methane was chosen as a model chemical system. The mechanism and kinetics of the thermal decomposition of methane have been the subject of many studies. Despite the fact that the gas-phase chemistry is relatively well understood, knowledge of surface processes is still incomplete. Experimental studies conducted by several investigators[16–18] have shown that the gaseous decomposition reaction is first order in methane concentration. These studies suggest that the process is limited by the initial rupture of the C–H bond. In the present work emphasis is placed on the effect of power modulation on the density evolution of the composite. Hence simplified chemical kinetics were used whereby the deposition of carbon is described by the following overall reaction:

$$CH_4 \rightarrow C + 2H_2 \tag{18}$$

The deposition rate is then given by

$$R_1^* = C_{CH_4} k_1 \exp\left[-E_1/(RT)\right] \tag{19}$$

The pre-exponential factor and activation energy were taken as $k_1 = 2.24 \times 10^{14}$ 1/s and $E_1 = 3.64 \times$

10^5 J/mole, respectively, close to the values reported by Kevorkian *et al.*[18] Despite its simplicity, Eq. (19) gave densification results in reasonable agreement with experimental data.[11] In accordance with Eq. (18), three gaseous components were included in the model, namely, methane, hydrogen, and argon (an inert).

D. Numerical method

The method of lines was used to solve the set of governing partial differential equations for the temperature, porosity, and species mole fractions (subject to the appropriate boundary and initial conditions). The technique of orthogonal collocation on finite elements with B-splines basis functions[19] was employed for the discretization of the spatial derivatives. The resulting set of ordinary differential equations was integrated in time using a variable-step variable-formula method. In order to capture the dynamics of the process, the maximum time step-size allowed did not exceed 2 s. The simulations reported in this study involved approximately 400 unknowns and were performed on a CRAY-YMP supercomputer. The CPU time needed to obtain the solution varied from 1 to 15 min, depending on the parameter values used.

III. RESULTS AND DISCUSSION

The results presented below show the behavior of pulsed-power volume-heating CVI as a function of key system variables, and pinpoint toward regions in the parameter space which may be more suitable for composite fabrication. In particular, the effect of power density, pulse period, duty cycle, and methane concentration on the deposit uniformity and densification time is elucidated. The values of transport and physical properties employed in the simulations are given in Table I. The values used for other system parameters are shown in Table II. These basic parameter values were used in the simulations unchanged unless otherwise stated. Power density is given in terms of a dimensionless quantity $\Phi^* = \Phi a^2/(Tk)_{\text{ref}}$ where Φ is the actual power, and T and k are reference temperature and thermal conductivity with values 1000 K and 6.58×10^{-2} J/(m s K), respectively.

TABLE I. Physical and transport properties.

$D_1^e = 12.11 w(\epsilon) d_p T^{0.5}$, m^2/s
$D_2^e = 34.16 w(\epsilon) d_p T^{0.5}$, m^2/s
$D_3^e = 7.67 w(\epsilon) d_p T^{0.5}$, m^2/s
$D_{12} = 1.224 \times 10^{-8}\, T^{1.5}/(P\Omega_{12})$, m^2/s
$D_{13} = 4.192 \times 10^{-9}\, T^{1.5}/(P\Omega_{13})$, m^2/s
$D_{23} = 1.337 \times 10^{-8}\, T^{1.5}/(P\Omega_{23})$, m^2/s
$M_1 = 16.04$ g/mol
$M_2 = 2.016$ g/mol
$M_3 = 39.944$ g/mol
$\rho_C = 1.74$ g/cm^3
$k_G = 4.516 \times 10^{-3}\, T^{0.5}$ J/(m s K)
$k_s^{-1} = 0.239(2.4 + 3.46 \times 10^{-3}\, T)$(m s K)/J
$k^e = (1 - \epsilon)^2 k_s + \epsilon^2 k_G$

TABLE II. Basic parameter values used for calculations.

Symbol	Name	Basic value
a	Preform radius	1 mm
$\epsilon_{A,0}$	Initial accessible porosity	0.5
Nu	Nusselt number	0.2
P_0	Initial pressure	1 atm
r_f	Fiber radius	4.0 μm
T_b	Ambient temperature	300 K
x_{1b}	Ambient methane mole fraction	0.6
x_{2b}	Ambient argon mole fraction	0.4

In order to isolate the effects of pulsed-power on the dynamics of CVI with volume-heating, a CVI process with a constant power volume-heating source is considered first. This process, examined in detail in Ref. 11, is also described by the aforementioned modeling equations except that Φ in Eq. (8) is independent of time. Figure 3 shows the spatial and temporal dependence of the accessible porosity for two values of the dimensionless power density, Φ^*. For the parameters used, a power value of 7.14 units corresponds to a power density of 4.7×10^8 W/m^3. Dimensionless positions of 0 and 1 correspond to the center and surface of the composite, respectively. The deposition process is characterized by an "inside-out" densification pattern in which a reaction zone develops at the center of the composite and moves toward the surface as time passes. This behavior is a direct consequence of the existing temperature profile in the composite which is maximum at the center and decreases monotonically toward the edges. Such a temperature distribution slows down the reaction rate close to the surface, thus allowing deep penetration of methane into the composite. For values of the dimensionless power density less than the critical value [Fig. 3(a)], the densification is completed without early pore closure resulting in a fiber-matrix composite with excellent density uniformity (the critical power is $\Phi_c^* = 7.6$ under these conditions). In order to reduce the processing time, one may increase the power input. However, for powers greater than the critical value, the process becomes controlled by diffusion leading to nonuniform deposition and the entrapment of accessible porosity within the composite [Fig. 3(b)].

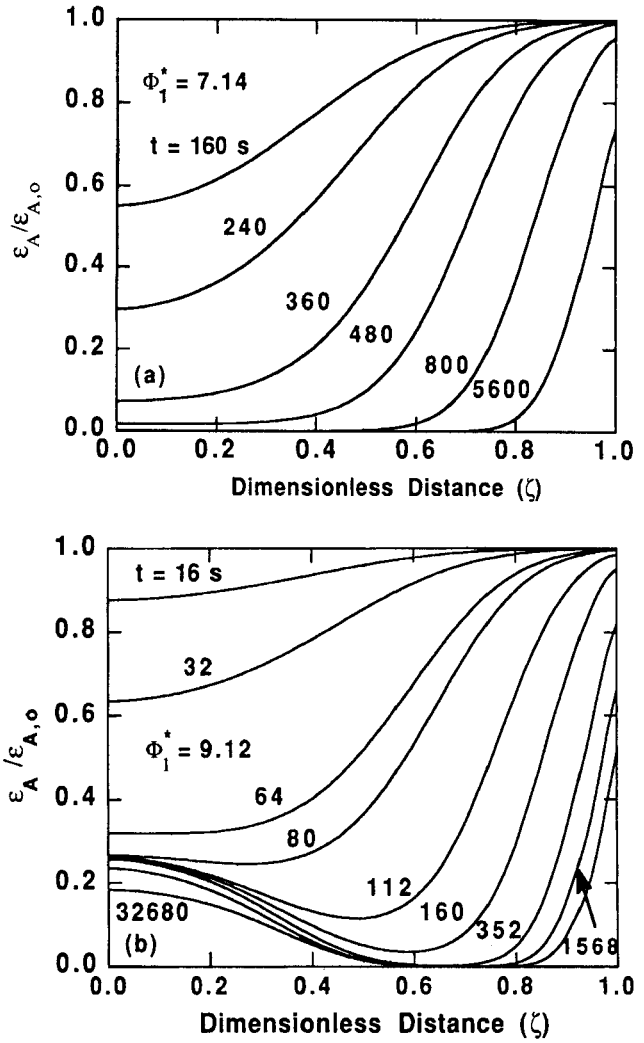

FIG. 3. Evolution of accessible porosity profiles for constant power volume-heating CVI for dimensionless power of (a) $\Phi^* = 7.14$ and (b) $\Phi^* = 9.12$.

These two cases are representative of the behavior of constant power volume-heating CVI. A similar behavior was observed by Sugiyama and Ohzawa[20] in SiC deposition using a pressure pulse CVI with RF heating. Their experimental results show that at 1273 K the deposition follows an "inside-out" densification pattern, but at higher temperatures (e.g., 1573 K) the deposition takes place primarily at the outer part of the composite. To overcome some of the unfavorable characteristics of the constant power process several power modulation schemes were suggested.[11] These schemes consisted of step changes in power at specific times during densification. In practice, however, it is difficult to determine the switching time(s) *a priori*. Therefore, pulsed-power volume-heating CVI is proposed in which the power is modulated according to a square-wave. This process is characterized by the dimensionless high-power and low-power values (Φ_1^* and Φ_2^*, respectively), the pulse period, t_p, and the duty cycle, f_d. In all simulations reported below power pulsing commences with the high power applied at time $t = 0$.

Figure 4 shows the variation of accessible porosity with position and time for pulsed-power volume-heating CVI. The pulse period is 180 s with a duty cycle of 50%. The high and low dimensionless powers are 9.12 and 7.14, respectively. One observes that the porosity profiles are qualitatively similar to the ones corresponding to constant power CVI, i.e., an "inside out" densification pattern. However, the processing time is shorter and the trapped porosity is less with the pulsed-power technique as compared to the constant-power CVI (Fig. 3). This result suggests that the pulsed-power volume-heating process has the potential of providing lower processing times without compromising the deposit uniformity.

To see the effect of duty cycle on the deposition process the case of $f_d = 25\%$ is examined, keeping all other parameters the same as in Fig. 4. The spatio-temporal variation of the accessible porosity is shown in Fig. 5. When compared to Fig. 4, the profiles illustrate a substantial decrease in trapped porosity with a corresponding increase in processing time. Because the duty cycle is lower, the composite now spends more time at lower temperatures leading to reduced diffusional limitations (hence denser composite) and also reduced reaction rates (hence longer processing time).

The enhanced density uniformity in pulsed-power volume heating CVI can be understood by looking at the evolution of the mole fraction profiles of methane and hydrogen. These are shown in Figs. 6(a) and 6(b) for times between 10^{-3} s and 40 s and 50 s to 170 s, respectively. The pulse period is 180 s and the duty cycle is 25%. Hence for the interval 0 s to 45 s the high power

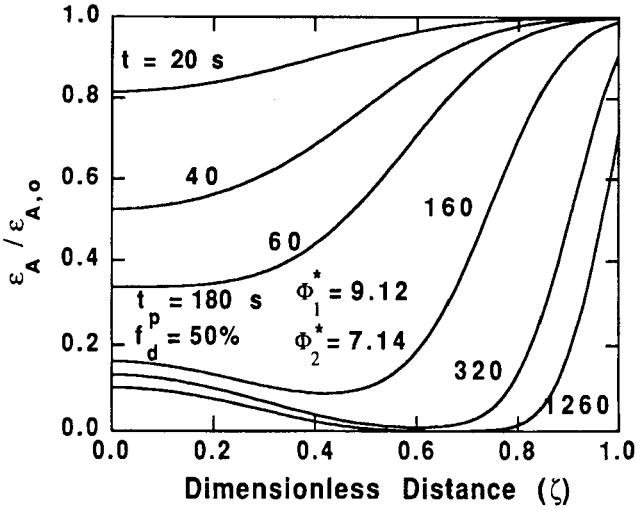

FIG. 4. Evolution of accessible porosity profiles for pulsed-power volume-heating CVI using dimensionless powers of $\Phi_1^* = 9.12$ and $\Phi_2^* = 7.14$. Duty cycle is 50% and pulse period is 180 s.

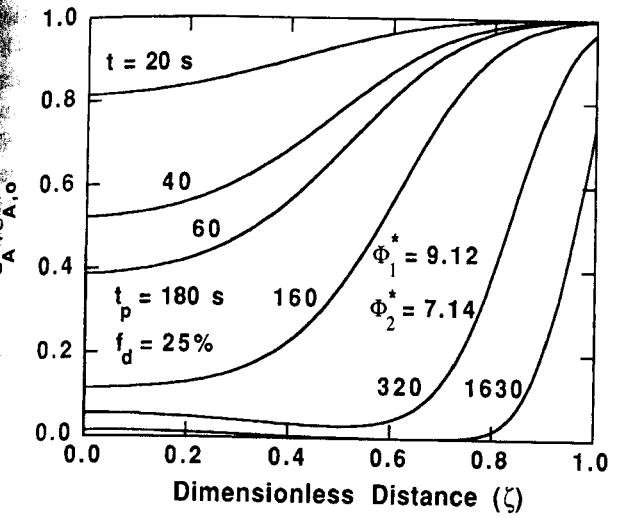

FIG. 5. Evolution of accessible porosity profiles for pulsed-power volume-heating CVI using dimensionless powers of $\Phi_1^* = 9.12$ and $\Phi_2^* = 7.14$. Duty cycle is 25% and pulse period is 180 s.

is on, and for the interval 45 s to 180 s the low power is on. During start-up and before the preform temperature is high enough for any chemical reaction to occur, methane diffuses rapidly into the preform, yielding a uniform reactant concentration profile. This happens on a time scale of 10 ms, equal to the characteristic diffusion time $\tau_d = \alpha^2/D$. As the preform heats up chemical reaction commences and a methane concentration gradient sets in [see Fig. 6(a) for $t = 10$ s]. This gradient becomes steeper as further reaction takes place during the high-power part of the cycle [i.e., for $t < 45$ s in Fig. 6(a)]. The associated hydrogen concentration profiles show that large amounts of byproduct are being accumulated in the core of the composite. The hydrogen mole fraction increases monotonically from the surface to the center of the composite and builds up as time advances. During the low-power part of the cycle the temperature and hence the methane decomposition rate drop. As a consequence, methane "refills" the interior of the composite [see profile for $t = 50$ s in Fig. 6(b)]. This replenishment of the reactant during the low-power part of the cycle is one of the advantages of pulsed-power volume-heating CVI. Another advantage stems from the fact that the deposition rate is kept high during the high-power part of the cycle. This can be seen clearly by comparing the change in porosity profiles in the intervals corresponding to 20–40 s and 40–60 s in Fig. 5. The high deposition rate minimizes the processing time.

The dynamic response of the center, T_c, surface, T_s, and spatially-averaged, T_{av}, temperature of the composite is shown in Fig. 7. The top portion of this figure shows the corresponding transient dependence of dimensionless power. The operating conditions are identical to those in Fig. 5. During start-up the preform temperature

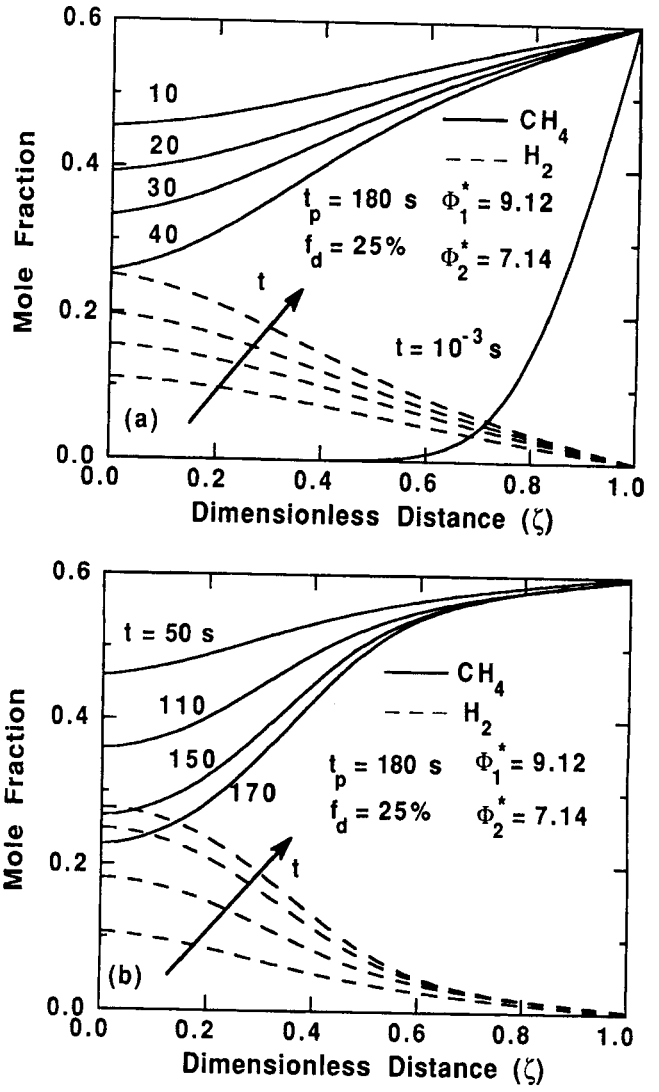

FIG. 6. (a) Spatiotemporal variation of CH_4 and H_2 mole fractions during the high-power part of the first cycle. Conditions as in Fig. 5. (b) Spatiotemporal variation of CH_4 and H_2 mole fractions during the low-power part of the first cycle. Conditions as in Fig. 5.

increases rapidly from its initial value of 300 K (the first period is not shown in Fig. 7), but essentially no reaction takes place until the temperature exceeds 1300 K. As expected, the power modulation leads to a periodic increase and decrease in the temperature of the composite. It is observed that the temperature follows closely the time dependence of power. As deposition progresses the porosity decreases continuously, resulting in higher values of thermal conductivity. Hence the heat generated in the composite can be transported easier to the surface of the composite from which it is lost by radiation and convection. This causes the mean of the temperature waveforms to drift to lower values as time passes. The spatiotemporal temperature variation induced by power pulsing may lead to development of significant thermal stresses in the composite. In general, the thermal stresses

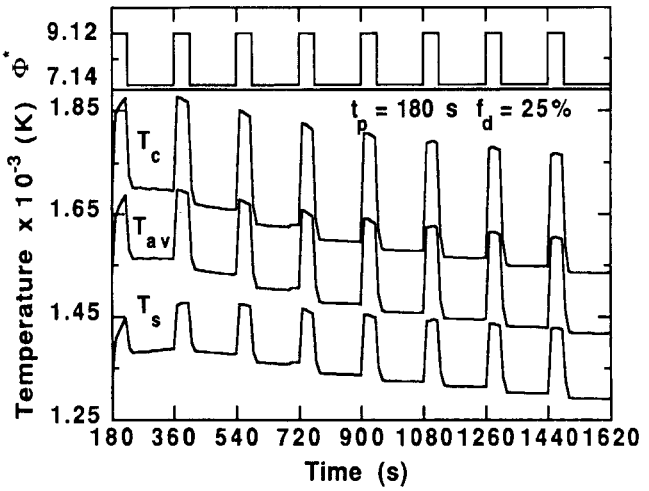

FIG. 7. Variation of the center, surface, and spatially-averaged temperatures as a function of time. Conditions as in Fig. 5. Top figure shows corresponding power modulation.

should be lower than the critical value above which fracture initiation or crack propagation can occur. Stress analysis is currently under investigation and will be presented elsewhere.

The dependence of the accessible porosity at the composite center, ϵ_{AC}, the average trapped accessible porosity, $\bar{\epsilon}_{A,T}$, and the processing time, $\tau_{10\%}$, on pulse period is shown in Fig. 8. The results are depicted for two values of the duty cycle. The processing time is the time required to reach an average accessible porosity of 10% of its initial value ($\bar{\epsilon}_A/\epsilon_{A0} = 0.1$). The porosity at the center of the composite is the highest value of residual porosity and, therefore, provides another useful criterion to assess density nonuniformities. In some cases the highest residual porosity may be the determining factor in choosing a particular set of operating conditions since it may lead to crack propagation in the composite. The general trends in Fig. 8 are as follows: (1) The average trapped porosity decreases with increasing pulse period and with decreasing duty cycle. Indeed, very low values of $\bar{\epsilon}_{A,T}$ can be obtained for a duty cycle of 25%. (2) The processing time increases by about 30% when the duty cycle is reduced from 50% to 25%. (3) At a duty cycle of 25% the processing time is not sensitive to the pulse period. (4) The center porosity decreases with increasing pulse period for 25% duty cycle, but goes through a minimum for 50% duty cycle. In addition, the center porosity decreases with decreasing duty cycle. The above trends underscore the complex dependence of CVI on important processing variables.

Figure 9 shows the variation of the average trapped accessible porosity, accessible porosity at the center, and processing time with duty cycle. The results are presented for a pulse period of 180 s and for two values of the preform radius, viz., $a = 1.0$ mm (solid lines) and $a = 1.25$ mm (dashed lines). A duty cycle of zero implies a constant dimensionless power of magnitude $\Phi_2^* = 7.14$, whereas a duty cycle of unity implies a constant power of $\Phi_1^* = 9.12$ (see Fig. 2). It is observed that both the average trapped porosity and the center porosity increase with increasing values of f_d. However, the dependence of $\epsilon_{AC}/\epsilon_{A,0}$ on f_d is more dramatic than that of $\bar{\epsilon}_{A,T}/\epsilon_{A,0}$, indicating that the entrapment of accessible porosity is confined to a small region at the center of the composite. These trends are a direct consequence of the higher temperatures prevailing in the composite as f_d increases, with correspondingly higher diffusional limitations. The processing time shows a significant decrease as f_d increases, followed by a plateau for values of f_d beyond 0.4. The trends are qualitatively similar for both radii, but $\tau_{10\%}$ is considerably larger whereas the trapped and center porosities are

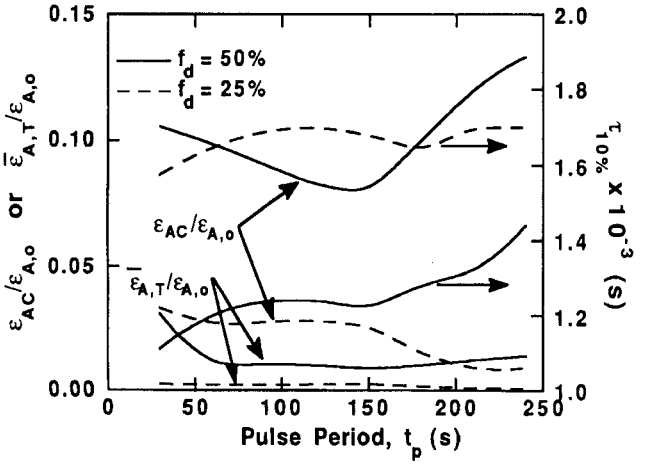

FIG. 8. Dependence of processing time, center accessible porosity, and average trapped accessible porosity on pulse period for two values of duty cycle. $\Phi_1^* = 9.12$ and $\Phi_2^* = 7.14$.

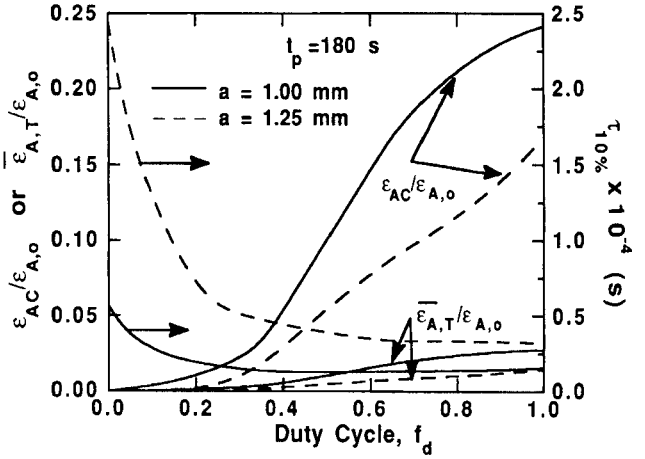

FIG. 9. Dependence of processing time, center accessible porosity, and average trapped accessible porosity on duty cycle for two preform radii. $\Phi_1^* = 9.12$ and $\Phi_2^* = 7.14$.

for the 1.25 mm-radius preform. Since identical ...ues for the dimensionless powers, Φ^*, were used for ...h composite radii, it becomes necessary to reduce ...actual power as a increases (see definition of Φ^*). ...wer values of power lead to lower temperatures and in ...lower reaction rate and lower diffusional limitations, ...ich explain the results obtained. Figure 9 suggests ...at best results in terms of rapid processing with little ...sidual porosity are obtained by operating with a duty ...cle of 25%, under the conditions examined.

The composition of the gaseous mixture is an im...portant parameter in CVI since it affects the deposition ...te and also the quality of the composite obtained. Results up to this point were for an ambient methane ...ole fraction of 60% with the remaining being argon. To explore the effect of methane concentration a mixture ...f 10% methane and 90% argon was also considered. The results are shown in Fig. 10 in terms of the same variables used in Fig. 9 and for two values of the pulse period. The average trapped and center porosities increase as f_d increases, a behavior similar to that seen in Fig. 9. The dependence of processing time on duty cycle, however, is considerably different from that observed in Fig. 9. As f_d increases, the processing time decreases sharply at first, goes through a minimum, and then increases with further increase of f_d. This can be explained in terms of the diffusion-reaction processes taking place in the composite. A duty cycle of zero corresponds to a constant power of 7.14 dimensionless units, which is below the critical power (see Ref. 11) and results in complete densification without any accessible porosity trapped. As f_d increases, the average temperature of the composite increases as well, resulting in higher deposition rate and shorter processing time without significant porosity entrapment. Further increase in f_d causes the process to become diffusion controlled, with a corresponding rise in both processing time and trapped porosity. At high values of the duty cycle the process is strongly controlled by the availability of methane inside the fiber-matrix composite. When compared with Fig. 9, the lower methane concentration leads to approximately a seven- to thirtyfold increase in processing time as the duty cycle increases from zero to unity. A close inspection of Fig. 10 shows that the best duty cycle in terms of optimizing processing time and deposit uniformity simultaneously appears to be around 20–25%. This is the same value found for the higher methane mole fraction in Fig. 9.

The choice of dimensionless power levels used so far in the pulsed-power scheme was based on the performance of the constant-power volume-heating study conducted previously. The stipulation was that the low power in the square-wave modulation scheme be lower than the critical value. This guarantees the existence of conditions that yield complete densification without the entrapment of otherwise accessible porosity. The low-power value chosen, $\Phi_2^* = 7.14$, satisfies that stipulation. However, the selection of the high power, Φ_1^*, used so far was partially arbitrary.

The dependence of the densification process on Φ_1^* was also investigated. Figure 11 shows the variation of the average trapped accessible porosity, the center accessible porosity, and the processing time on Φ_1^* for two values of methane mole fraction. For a 60% methane mole fraction (solid lines) the processing time decreases monotonically with increasing Φ_1^* while the residual porosities remain at very low values. The results for a 10% methane mole fraction show a more complex dependence of $\epsilon_{AC}/\epsilon_{A,0}$ and $\tau_{10\%}$ on Φ_1^*. It is observed that the processing time can be reduced by more than

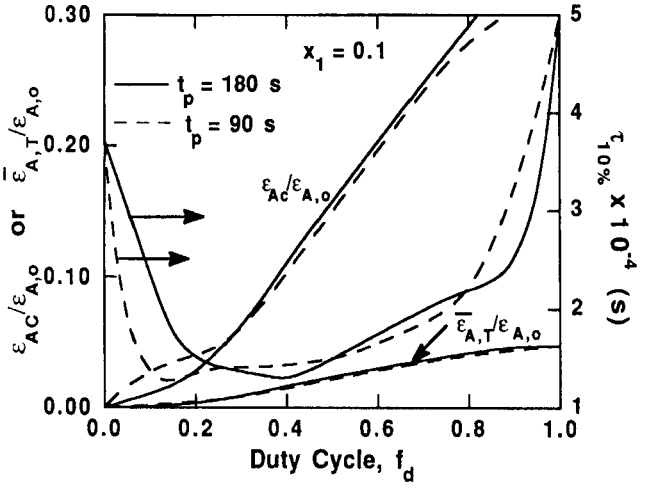

FIG. 10. Dependence of processing time, center accessible porosity, and average trapped accessible porosity on duty cycle for two values of pulse period. $\Phi_1^* = 9.12$, $\Phi_2^* = 7.14$, and methane mole fraction is 0.1.

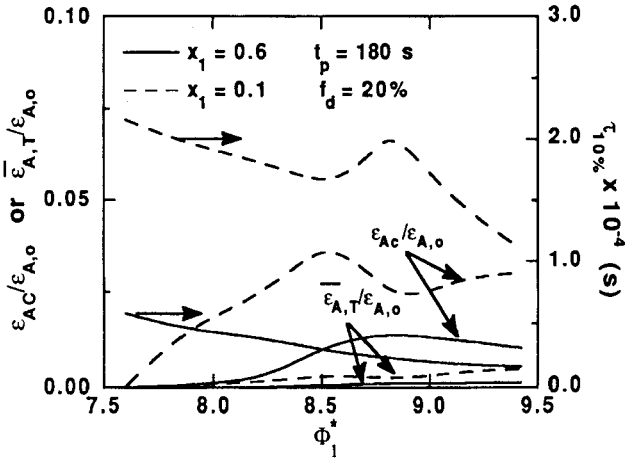

FIG. 11. Dependence of processing time, center accessible porosity, and average trapped accessible porosity on high power for two values of methane mole fraction. $t_p = 180$ s, $f_d = 20\%$, and $\Phi_2^* = 7.14$.

a factor of 2 when the high-power value increases from 7.5 to 9.4. At the same time the center porosity remains below 2.5%.

IV. SUMMARY AND CONCLUSIONS

A comprehensive mathematical model has been developed for a novel chemical vapor infiltration process called pulsed-power volume-heating CVI. In this technique, a volume-heating source (e.g., RF or microwave) is used to heat the preform. The source power is modulated in time (e.g., square-wave modulation) with a specific period and duty cycle. The general features of pulsed-power volume-heating CVI were illustrated by modeling the fabrication of a carbon-carbon composite using methane as a precursor gas. The densification process was described by a set of partial differential equations for the spatiotemporal variations of the species concentration, temperature, and porosity. The multicomponent transport processes were incorporated into the mathematical formulation using a rigorous explicit form of the Dusty Gas model.

The pulsed-power volume-heating technique was found to have the following beneficial attributes: (1) Volume-heating yields a temperature which is highest at the composite center and decreases monotonically toward the edges. This temperature profile results in slower reaction near the surface of the composite and deeper penetration of the reactant. (2) During the low-power part of the cycle the temperature of the composite drops, reducing the reaction rate and thus allowing the precursor gas to diffuse into the composite, essentially "refilling" the composite. The above two attributes alleviate reactant concentration gradients within the composite minimizing density nonuniformities. (3) During the high-power part of the cycle the deposition rate is rapid, thereby minimizing processing time.

A square-wave modulation scheme was employed. The effect of duty cycle, pulse period, power levels, and methane concentration on densification uniformity and processing time was examined. The results revealed that the duty cycle and pulse period have a substantial effect on the dynamics of the process. A window of operating conditions was identified which may be most beneficial for CVI. In particular, a duty cycle of 25% appeared best for the cases studied. Furthermore, it was found that lower methane mole fractions result in longer processing time by exacerbating diffusional limitations. The actual methane mole fraction, however, may be dictated by deposit quality considerations.

CVI is a complex process in the sense that the space and time variations of species concentration, temperature, and porosity of the composite interact strongly to influence the system behavior. Because of these complexities, the process is difficult to understand using intuition alone. Mathematical models can be used for gaining a better understanding of the process, for screening process alternatives, and for evaluating novel CVI techniques. In addition, the models can be used to pinpoint the window of operating conditions which may be optimum for the fabrication of ceramic composites.

LIST OF SYMBOLS

a	preform radius, m
A_r	defined by Eq. (3)
B_0	permeability of composite, m^2
C	gas concentration, kmol/m^3
C_{pr}	heat capacity of the rth gaseous species, kJ/(kmol K)
C_p^e	effective heat capacity of the composite, kJ/(m^3 K)
d_p	average pore diameter, m
D_r	Knudsen diffusion coefficient of the rth gaseous species, m^2/s
D_{rs}	binary diffusion coefficient of the r-s pair, m^2/s
E_i	activation energy of the ith reaction, kJ/kmol
f_d	duty cycle
h	heat transfer coefficient, kJ/(m^2 s K)
$\mathbf{J}_r$	molar flux of the rth species relative to the molar average velocity, kmol/(m^2 s)
k^e	effective thermal conductivity of the composite, kJ/(m s K)
M_r	molecular weight of the rth species, kg/kmol
$\mathbf{N}$, $\mathbf{N}_r$	total molar flux and molar flux of the rth species, respectively, kmol/(m^2 s)
Nu	Nusselt number (ha/k)
n^G, n^R, n^S	number of gaseous species, reactions, and solid species, respectively
P	pressure, atm
r	radial coordinate, m
R	gas constant, m^3 atm/(kmol K)
R_i	rate of the ith reaction per unit volume of composite, kmol/(m^3 s)
t	time, s
t_p	pulse period, s
t_1, t_2	interval of time in which the high or low power is on, s
T	temperature, K
$w(\epsilon)$	Knudsen flow polynomial (defined in Ref. 11)
x_r	mole fraction of the rth species
Greek	
ΔH_i	heat of the ith reaction, kJ/kmol

	defined by Eq. (5), m^2/s
	total porosity
	accessible porosity
	trapped accessible porosity
	emissivity of carbon
	dimensionless distance (r/α)
	viscosity of the gaseous mixture, kg/m s)
ν_{ri}	stoichiometric coefficient for species r in reaction i
ρ_C	density of deposited carbon, kg/m^3
σ	Stefan–Boltzmann constant, $kJ/(m^2\ s\ K^4)$
τ_d	dimensionless difusion time (tD/α^2)
$\tau_{10\%}$	processing time, s
Φ	power density of volume-heating source, W/m^3
Φ^*	dimensionless power density, $\Phi\alpha^2/(Tk)_{ref}$

Subscripts

0	initial value
b	bulk or ambient value
$r(r = 1,2,3)$	CH_4, H_2, and Ar, respectively
C	carbon

Superscript

e	effective value

ACKNOWLEDGMENT

The authors are grateful to the Pittsburgh Supercomputer Center (supported by NSF) for making computer time available on the CRAY-YMP supercomputer.

REFERENCES

1. M. A. Karnitz, D. F. Craig, and S. L. Richlen, Am. Ceram. Soc. Bull. **70**, 430 (1991).
2. J. A. Cornie, Y-M. Chiang, D. R. Uhlmann, A. Mortensen, and J. M. Collins, Am. Ceram. Soc. Bull. **65**, 293 (1986).
3. J. R. Strife, J. J. Brennan, and K. M. Prewo, Ceram. Eng. Sci. Proc. **11**, 871 (1990).
4. T. M. Besmann, R. A. Lowden, B. W. Sheldon, and D. P. Stinton, in *Chemical Vapor Deposition,* edited by K. E. Spear and G. W. Cullen (The Electrochemical Society, Pennington, NJ, 1990), p. 482.
5. S. Middleman, J. Mater. Res. **4**, 1515 (1989).
6. B. W. Sheldon, J. Mater. Res. **5**, 2729 (1990).
7. R. R. Melkote and K. F. Jensen, in *Chemical Vapor Deposition of Refractory Metals and Ceramics,* edited by T. M. Besmann and B. M. Gallois (Mater. Res. Soc. Symp. Proc. **168**, Pittsburgh, PA, 1990), p. 67.
8. S. V. Sotirchos, AIChE J. **37**, 1365 (1991).
9. W. H. Sutton, Am. Ceram. Soc. Bull. **68**, 376 (1989).
10. D. Gupta and J. W. Evans, J. Mater. Res. **6**, 810 (1991).
11. J. I. Morell, D. J. Economou, and N. R. Amundson, J. Electrochem. Soc. **139**, 328 (1992).
12. R. Jackson, *Transport in Porous Catalysts* (Elsevier Publishing Company, New York, 1977).
13. R. R. Melkote and K. F. Jensen, AIChE J. **35**, 1942 (1989).
14. M. M. Tomadakis and S. V. Sotirchos, AIChE J. **37**, 74 (1991).
15. R. B. Bird, W. E. Stewart, and E. N. Lightfoot, *Transport Phenomena* (John Wiley & Sons, New York, 1960).
16. H. B. Palmer and T. J. Hirt, J. Phys. Chem. **67**, 709 (1963).
17. G. B. Skinner and R. A. Ruehrwein, J. Phys. Chem. **63**, 1736 (1959).
18. V. Kevorkian, C. E. Heath, and M. Boudart, J. Phys. Chem. **64**, 964 (1960).
19. C. de Boor, *A Practical Guide to Splines* (Springer-Verlag, New York, 1978).
20. K. Sugiyama and Y. Ohzawa, J. Mater. Sci. **25**, 4511 (1990).